Matematisk-fysiske Meddelelser
udgivet af
Det Kongelige Danske Videnskabernes Selskab
Bind **35,** nr. 10

Mat. Fys. Medd. Dan. Vid. Selsk. **35,** no. 10 (1966)

STOPPING CROSS SECTION IN CARBON OF 0.1-1.0 MeV ATOMS WITH $6 \leq Z_1 \leq 20$

BY

B. FASTRUP, P. HVELPLUND AND C. A. SAUTTER

København 1966
Kommissionær: Munksgaard

Synopsis

The stopping cross section, $\frac{1}{N}\frac{dE}{dx}$, in thin carbon foils has been measured for ions, $6 \leq Z_1 \leq 20$, with energies from 100 kev to 1 Mev. The experimental data have been corrected numerically for nuclear stopping to obtain the electronic stopping. The electronic stopping cross section has an oscillatory dependence on the atomic number, Z_1, for constant ion velocities. The analysis suggests that the relative amplitude of the oscillations decreases as the ion velocities increase. Apart from the oscillations, the experimental data are in reasonable agreement with the theoretical predictions. The relative accuracy of the measured data is about 2–3 per cent, and the absolute accuracy of the evaluated electronic stopping cross sections is better than 8 per cent even in the most extreme cases (low energy and high Z_1).

PRINTED IN DENMARK
BIANCO LUNOS BOGTRYKKERI A/S

Introduction

The basis for a theoretical description of the energy loss of heavy ions penetrating matter was laid by BOHR[1]. In his treatment, the stopping process is due to two distinct mechanisms: inelastic collisions with the electrons of the target atom, and elastic collisions with the target atom as a whole. The inelastic processes are dominant at high velocities, $v \gg v_0^*$, where the well-known Bethe-Bloch formula applies, while the elastic processes are almost completely responsible for the slowing-down of the ion at low velocities, $v \lesssim v_0$. However, theoretical studies of an electron gas by FERMI and TELLER[2] and by LINDHARD[3] indicate a non-vanishing electronic stopping component even at low velocity.

Unlike chemical reactions, atomic collision processes are quite violent disturbances of atoms, so the effects due to atomic shell structure, chemical properties, charge exchange, etc., should normally be of secondary importance for heavy ions. This makes it attractive to apply statistical methods as a basis for theoretical studies. FIRSOV[4] and LINDHARD and SCHARFF[5] have used Thomas-Fermi arguments to evaluate the electronic stopping cross section at low velocity, and the over-all agreement with experimental results is good.

Employing the Thomas-Fermi arguments, Lindhard and Scharff obtained for the electronic stopping cross section

$$S_e = \xi_e \frac{8\pi e^2 a_0 Z_1 Z_2}{Z} \frac{v}{v_0}, \quad (Z^{2/3} = Z_1^{2/3} + Z_2^{2/3})$$

valid for projectile velocities v less than $v_0 Z_1^{2/3}$. Here, ξ_e is a constant of order $1-2$ which may vary approximately as $Z_1^{1/6}$.

Recently, ORMROD et al.[6] have subjected the Lindhard theory of electronic stopping to a systematic experimental test in carbon and aluminum films at low energy, $E \leq 140$ kev. Although the over-all agreement with theory is reasonably good, they found a striking oscillatory behaviour of

* v_0 is the electron velocity in the first Bohr orbit of hydrogen.

S_e as a function of Z_1 for a common projectile velocity $v \sim 0.41\, v_0$. It is tempting to associate these periodic deviations with the atomic shell structure of the penetrating ions. However, quantitative theoretical calculations have not yet been made.

As the heavy-ion accelerator at the University of Aarhus[7] is well-suited for the production of ions of nearly all elements with energies up to approximately 1 Mev (doubly charged ions), it was decided to extend further the empirical information of the stopping process of heavy ions in carbon films. It was of particular interest to study the oscillation of S_e at even higher projectile velocities where it is expected that the shell structure of the ions is less important*.

Apparatus

The Aarhus 600-kv heavy-ion accelerator, provided with a universal ion source, furnished the projectiles for these experiments. By means of (p,γ) resonances in F^{19} and Al^{27} targets and a (p,α) resonance in a B^{11} target, a preliminary energy calibration was carried out.

Figure 1 shows a schematic diagram of the experimental set-up. After acceleration and deflection in the bending magnet, the ion beam is parallel-collimated by movable apertures (a) and (b) to within 1/3 degree. At the entrance and the exit ports of the target chamber, in which the films are situated, liquid-air traps are fitted to minimize the build-up of any surface contamination. The operating pressure in the target chamber is 10^{-5} Torr or less.

Attached to the target chamber is a special film holder enabling interposition of one or several (up to eight) areas of two different films in the path of the particles at the objective position of the analyzing magnet. With this device, the position of a film can be reproduced for successive ion bombardments.

The beam path in the accelerator is horizontal, whereas the plane of the deflection in the analyzer is vertical. The analyzer is a 90° sector magnet with two-directional focusing obtained by the use of inclined pole piece edges.

* Recent range studies at this Institute by J. A. Davies, L. Eriksson, and P. Jespersgaard, the results of which have been published (in part) in Nucl. Instr. Meth. *38* (1965) 245, have shown the same type of oscillations of S_e. In their experiment, an oriented tungsten monocrystal was bombarded by ions with Z_1 = 11, 15, 18, 19, 24, 29, 35, 36, 37, 54, and 55 at energies between 70 kev and 1500 kev. Due to channeling, the nuclear stopping was negligible compared with the electronic stopping.

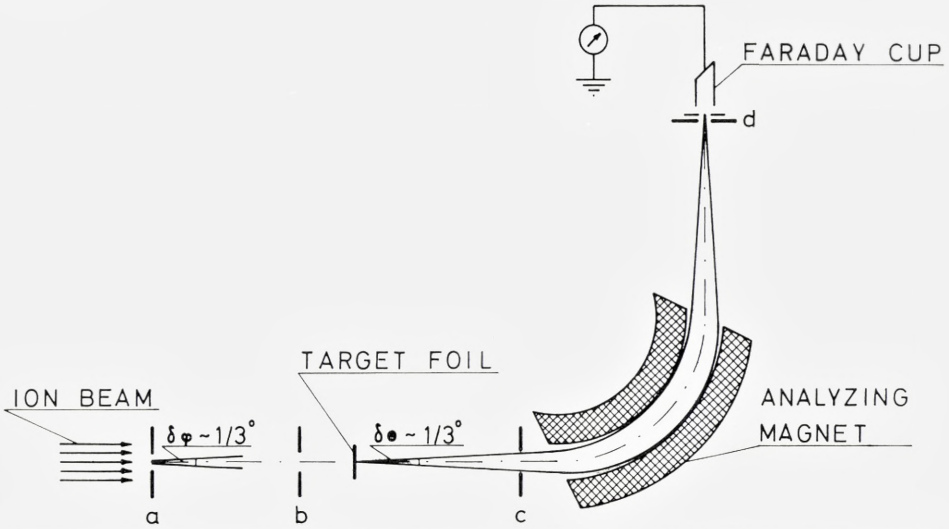

Fig. 1. The experimental arrangement. a), b), c), and d) indicate the limiting apertures in the set-up.

The entrance slit to the Faraday-cup detector at (d) is approximately 5 mm wide and perpendicular to a plane which contains the trajectories of the ions through the analyzer, providing an energy resolution $\Delta E/E$ better than 0.5 per cent.

For the measurement of the relative changes in the magnetic field of the analyzer, which we use to determine energy losses, an instrument incorporating a Hall element with linearity better than 0.2 per cent was constructed.

Experimental Method

The energy loss suffered by protons penetrating the carbon film is used to determine the film thickness. The thicknesses ranged from about $6\,\mu g/cm^2$ to $23\,\mu g/cm^2$ for the films used in the heavy-ion experiment. In order to make a preliminary calibration of this technique, two thicker films ($\sim 30\,\mu g/cm^2$) of known areas were weighed on a microbalance to about $\pm 1\,\mu g$. Subsequently, a mean energy loss was obtained for 150-kev protons for each of these two films. Energy loss measurements were made on four different areas of both films.

The 150-cm radius 75° sector bending magnet is used to define the mass of the projectiles entering the target chamber. With no film in the path of the ion beam, the projectiles are deflected by the field of the analyzing magnet into the Faraday-cup detector (refer to Fig. 1). Both with and without the film placed in the beam path, the analyzer field is adjusted for maximum response at the Faraday-cup detector with respect to the energy distribution profiles. The width of the incident beam energy profile is almost completely accounted for by the combined resolution of the analyzer and the slit at the detector.

In this experiment we measure the most probable energy loss, ΔE_0, defined as the difference between the energies of the maxima of the incident and the emerging beam profiles. The observed stopping cross section per atom, S_0, is then assumed to be given by the relation

$$S_0 = \frac{1}{N}\frac{\Delta E_0}{\Delta R}$$

at the mean energy $\bar{E} = E_i - \Delta E_0/2$, where E_i is the energy of the projectiles incident upon a film. Here, N is the number of carbon atoms per unit volume, and ΔR is the film thickness. In all cases reported here, the ratio $\Delta E_0/\Delta R$ is a good approximation to $-dE/dR$.

We determine ΔE_0 by the following technique, based on the assumption that the energy E of the beam transmitted by the magnetic analyzer is related to the field B of the analyzer, by the equation $E = kB^2$, where k is a constant. Employing this relation, we have

$$\Delta E_0 = E_i(2 - \Delta B/B_i)\Delta B/B_i,$$

where B_i is the analyzer magnetic field corresponding to the peak E_i in the energy distribution without film, and $\Delta B/B_i$ is the corresponding relative reduction in magnetic field for the transmitted beam. We then obtain

$$S_0 = \frac{A_2 E_i}{N_0 \Delta x}\frac{\Delta B}{B_i}\cdot(2 - \Delta B/B_i),$$

where N_0, Δx, and A_2 are Avogadro's number, the film surface density in grams/cm^2, and the gram-atomic weight of carbon, respectively.

Data Treatment

The electronic stopping cross section S_e is obtained by subtracting the nuclear stopping cross section S_n^* from the observed stopping cross section S_0, i.e.

$$S_e = S_0 - S_n^*.$$

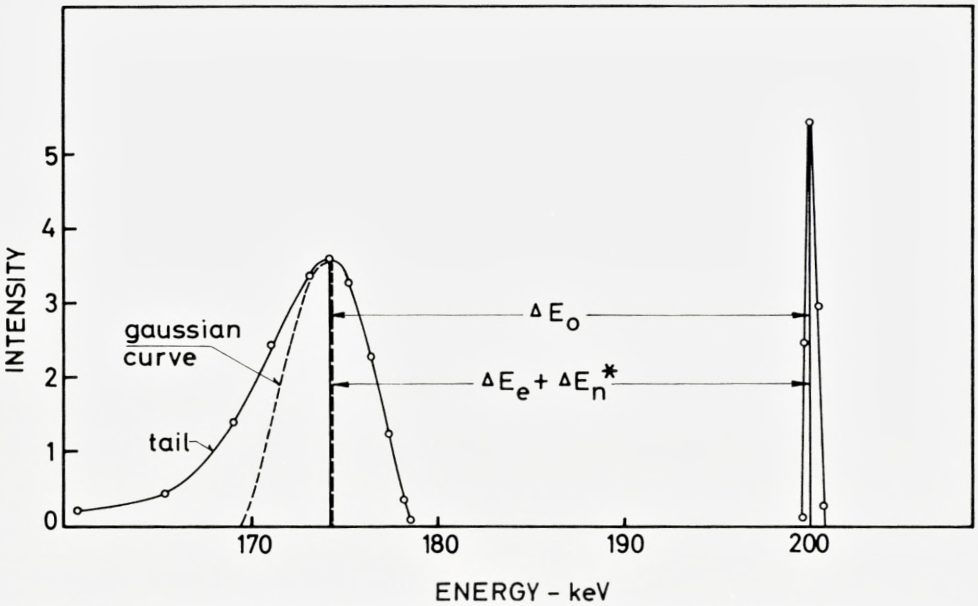

Figure 2. Energy distribution of Ar^{40} ions emerging from a 6.7 $\mu g/cm^2$ carbon film through the aperture in front of the magnet. The energy of incident ions is 200 kev.

The energy profile of the beam emerging from a foil consists of two parts: a Gaussian distribution due to soft collisions, and a tail resulting from violent ones. According to BOHR[1] and WILLIAMS[8], we may assume that the Gaussian distribution accounts almost exclusively for the peak position of the observed distribution, whereas violent collisions result in anomalously large energy losses and add to the tail only, see Fig. 2.

The most probable energy loss of the ions traversing the foil corresponds to the sum of the mean electronic energy loss, ΔE_e, and the most probable nuclear energy loss, ΔE_n^*, i.e.

$$\Delta E_0 \simeq \Delta E_e + \Delta E_n^*.$$

Here,

$$\Delta E_n^* = N\Delta R \int_0^{T_1^*} T d\sigma ,$$

where $N\Delta R$ is the number of atoms per cm^2 and $d\sigma$ is the differential cross section for an energy transfer T.

According to BOHR[1], T_1^* is roughly equal to the standard deviation of the Gaussian nuclear energy loss distribution, Ω_n^*, i.e.

$$(T_1^*)^2 \approx (\Omega_n^*)^2 \approx N\Delta R \int_0^{T_1^*} T^2 d\sigma, \text{ provided } \Delta E_0 \ll E_i .$$

As shown in the Appendix, the nuclear stopping cross section S_n^* is found to be

$$S_n^* = \int_0^{T_1^*} T d\sigma = 2.57 \cdot 10^{-16} \frac{A_1 Z_1^2 Z_2^2 \varepsilon^*}{A_2 E} I(\varepsilon^*) \text{ ev} \cdot \text{cm}^2/\text{atom},^* \qquad (1)$$

where $I(\varepsilon) = \dfrac{d\varepsilon}{d\varrho}$ (the nuclear stopping cross section in reduced units[5]), E is measured in kev, and ε^* is derived from the equation

$$F(\varepsilon^*) = \frac{\int_0^{\varepsilon^*} x^2 f(x) dx}{(\varepsilon^*)^4} = \frac{1}{N\Delta R \pi a^2}$$

The function $F(\varepsilon^*)$ has been calculated numerically by using the Thomas-Fermi differential scattering cross section[9]. The result is shown in Fig. 3.

So far, the effect of the small acceptance angle of the analyzing magnet has not been considered. The energy profile of the particles emerging from the foil within the acceptance angle is different from the energy profile of

* In the present experiment, T_1^* is always much smaller than the maximum energy transfer $T_{\max} = 4M_1M_2E/(M_1+M_2)^2$, and hence S_n^* is much smaller than the total nuclear stopping cross section $S_n = \int_0^{T_{\max}} T d\sigma$. For example, in the case of 90 kev Ar ions penetrating a 7.5 $\mu g/\text{cm}^2$ carbon foil, the ratio between T_1^* and $T_{\max}$ is approx. 0.025, and the nuclear stopping cross section, S_n^*, corresponding to the peak of the Gaussian nuclear energy loss, is only one fifth of the total nuclear stopping cross section, S_n.

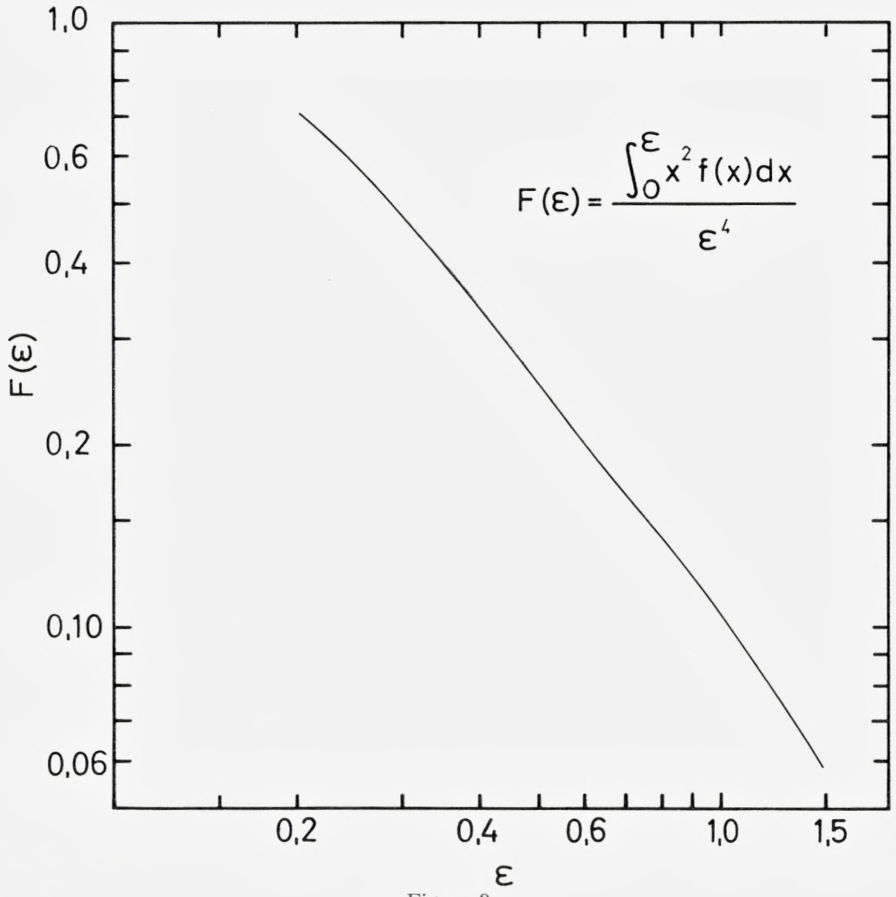

Figure 3.

all particles emerging from the foil. Particles which have experienced violent collisions with target atoms are scattered out of the acceptance angle and do not contribute to the observed energy loss distribution.

To see that the nuclear energy loss formula, eq. (1), is still valid in the case of a small acceptance angle, we must show that although the tail may be radically changed, the Gaussian nuclear energy loss distribution is unaffected.

The multiple scattering (angular) distribution of the particles emerging from the foil, see Fig. 4, is divided into a Gaussian peak and a tail. Collisions with individual deflection angles φ less than φ^* produce the Gaussian

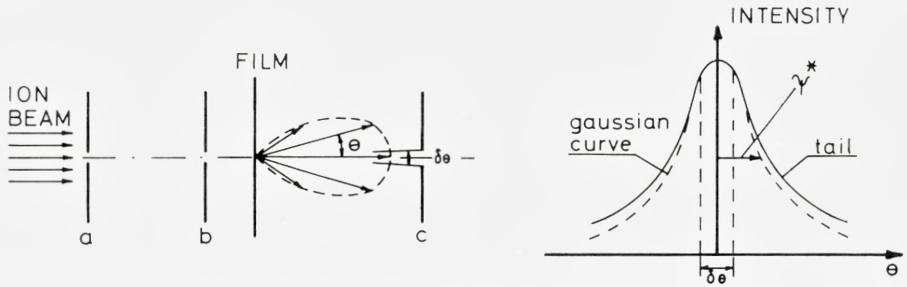

Figure 4. The angular distribution of ions emerging from the foil. $\delta\theta$ indicates the acceptance angle of the analyzing magnet.

distribution and account for the angular distribution for angles θ smaller than the half-width Ψ^* of the Gaussian distribution. Collisions with deflection angles larger than φ^* produce a tail distribution which prevails for θ larger than Ψ^*.

The acceptance angle of the analyzing magnet $\delta\theta$ is much smaller (one tenth) than the width Ψ^*.

A good first order estimate of φ^* is the half-width of the Gaussian distribution, i.e.

$$(\varphi^*)^2 \approx (\Psi^*)^2 \approx N\Delta R \int_0^{\varphi^*} \varphi^2 d\sigma, \tag{2}$$

where $d\sigma$ is the differential scattering cross section for an angular deflection φ.

For $\varphi^* \ll 1$, which is normally fulfilled, $(\varphi^*)^2 \approx A_2 T_2^*/(A_1 E)$, where T_2^* is the maximum energy transfer to the target atoms in a single collision with the ions admitted to the analyzing magnet, and A_1 and A_2 are atomic weights of the projectile and the target, respectively. In fact, T_2^* is the maximum energy transfer if the multiple scattering angle θ is smaller than approximately Ψ^*.

If, for instance, the differential scattering cross section for a Thomas-Fermi potential[5] is used, eq. (2) may be solved with respect to φ^* and T_2^*.

In all cases reported here, it turns out that $T_2^* \gg T_1^*$; in fact $T_2^* \approx 7T_1^*$, which confirms the choice of T_1^* as the upper limit in the integral in eq. (1). This partly explains how the observed energy loss distribution may be asymmetric. Cases where the ions have experienced two or more violent collisions and reappear in the forward direction will also contribute to the tail.

From the collected data, measurements with a nuclear correction larger than 25 per cent of the observed stopping cross section have been discarded. It is believed that possible errors in the estimate of S_n^* are less than 20 per cent which result in a systematic error no greater than 4–5 per cent even in the most extreme cases (low energy and high Z_1).

The small acceptance angle eliminates possible discrepancies between projected path and actual path; hence no correction has been applied.

Results and Discussion

In the table on pp. 12–13 are given the results of the measurements, including the electronic stopping cross sections which are extracted in the manner previously described. It should be recalled that all these data are based upon a determination of the absolute stopping cross section of carbon for 150-kev protons, the result of which is

$$S_0 = S_e = 12{,}6 \times 10^{-15} \text{ ev} \cdot \text{cm}^2/\text{atom} \pm 3 \text{ per cent.}$$

This value differs by less than 1 per cent from that obtained by SAUTTER and ZIMMERMANN[10], but is 9 per cent lower than that reported by MOORHEAD[11].

In order to adjust the measured data to each other, an intercalibration measurement was performed. At 400 kev, stopping power data were taken for all Z_1-values with two carbon films, the thicknesses of which were determined in the same run. As a result of the intercalibration, it was found that only two stopping curves had to be renormalized more than 3 per cent. In the cases of Ar^{40} and K^{39}, the original curves were raised 6 per cent and lowered 6 per cent, respectively.

The change of the film thickness during irradiation was carefully studied by comparing the energy loss of 150-kev protons before and after the irradiation. In no cases did the change exceed a few per cent.

The relative accuracy of the measured total stopping data is established within 2–3 per cent. The absolute values of the electronic stopping cross sections are estimated to be better than 8 per cent. This estimate includes errors in proton stopping values at 150 kev, and nuclear stopping corrections.

The agreement with both higher- and lower-energy empirical data is reasonably good. In all but one instance, the present data smoothly fill the intermediate energy region. In the case of C^{12}, N^{14}, O^{16}, and Ne^{20} projectiles, information is provided both by the work of PORAT and RAMAVATARAM[12] at energies above 360 kev, and of ORMROD et al.[6] at energies below

TABLE: Stopping cross sections in carbon for the atoms indicated at various energies. The foil thicknes is denoted Δx; column a) is S_n^*, the computed nuclear stopping, and column b) is the derived electronic stopping, both in units of 10^{-14} ev · cm^2/atom.

Atom	E (kev)	Δx (μg/cm^2)	a)	b)	Atom	E (kev)	Δx (μg cm^2)	a)	b)
C^{12}	82	14.7	0.12	3.89	Na^{23}	90	7.98	0.40	2.65
–	131	14.5	0.08	4.85	–	134	14.7	0.42	3.15
–	180	14.9	0.06	5.47	–	182	15.4	0.31	3.82
–	232	14.7	0.04	6.10	–	283	15.4	0.20	4.85
–	282	14.5	0.04	6.41	–	377	21.0	0.20	5.91
–	381	14.7	0.02	7.44	–	468	20.0	0.15	6.88
					–	592	9.67	0.07	8.31
N^{14}	73	22.7	0.28	3.90	–	758	19.9	0.09	9.68
–	121	22.7	0.16	4.75	–	898	6.90	0.04	10.35
–	172	21.6	0.12	5.42					
–	220	22.1	0.09	6.13	Mg^{25}	135	13.2	0.50	3.00
–	270	22.1	0.08	6.65	–	185	13.2	0.36	3.64
–	320	21.6	0.06	7.10	–	236	15.3	0.30	4.41
–	418	21.4	0.05	7.85	–	286	15.3	0.26	4.97
					–	375	22.5	0.25	5.77
O^{16}	81	15.2	0.29	3.85	–	572	21.6	0.16	7.33
–	131	14.8	0.18	4.94	–	766	21.6	0.12	9.34
–	180	15.1	0.14	5.44					
–	231	15.1	0.10	6.04	Al^{27}	88	9.12	0.70	2.78
–	282	15.2	0.08	6.38	–	140	9.34	0.47	3.53
–	330	15.2	0.07	6.96	–	182	15.4	0.48	4.10
–	380	15.1	0.06	7.42	–	292	10.0	0.24	5.52
–	430	15.1	0.06	7.82	–	464	24.1	0.25	7.21
–	479	15.1	0.05	8.27	–	563	19.5	0.18	8.17
					–	658	24.1	0.19	9.20
F^{19}	138	9.55	0.18	4.20	–	777	11.8	0.10	9.86
–	189	9.55	0.13	4.78	–	875	11.8	0.10	10.57
–	291	9.55	0.09	6.04					
–	370	23.1	0.12	6.52	Si^{28}	133	13.2	0.72	3.78
–	473	15.8	0.08	7.32	–	182	13.2	0.52	4.42
					–	288	12.0	0.31	5.94
Ne^{20}	81	18.8	0.61	2.76	–	386	12.1	0.24	6.94
–	133	14.2	0.32	3.75	–	582	13.9	0.18	8.91
–	183	16.6	0.25	4.32	–	780	13.9	0.14	10.5
–	285	15.2	0.16	5.44					
–	379	18.0	0.13	6.48	P^{31}	137	9.42	0.70	4.24
–	482	15.2	0.09	7.16	–	188	9.42	0.52	4.99
–	562	20.7	0.09	8.15	–	291	9.16	0.32	6.40
–	755	20.7	0.07	10.00	–	363	23.5	0.50	7.44
–	946	20.7	0.06	11.62	–	460	23.4	0.40	8.12

TABLE (continued).

Atom	E (kev)	Δx (μg/cm^2)	a)	b)	Atom	E (kev)	Δx (μg/cm^2)	a)	b)
P^{31}	557	19.8	0.29	9.30	Ar^{40}	394	7.28	0.36	8.42
–	654	23.8	0.28	10.09	–	492	7.75	0.29	9.12
–	849	23.7	0.22	11.58	–	593	7.75	0.24	9.98
					–	695	7.48	0.20	10.63
S^{32}	168	21.5	1.16	5.17	–	797	7.40	0.18	11.16
–	265	22.0	0.76	6.70	–	996	19.6	0.28	12.50
–	314	22.1	0.64	7.32	–	1163	19.6	0.24	13.11
–	556	22.4	0.36	9.77	–	1290	20.0	0.24	13.60
–	753	22.5	0.28	11.06					
					K^{39}	138	6.94	1.03	5.27
Cl^{35}	134	10.9	1.11	4.66	–	190	6.05	0.66	6.25
–	184	10.9	0.80	5.62	–	292	6.83	0.47	7.49
–	236	10.3	0.62	6.41	–	393	6.55	0.33	8.90
–	283	12.2	0.58	7.04	–	466	15.3	0.54	9.10
–	362	22.1	0.68	7.73	–	594	6.55	0.23	10.40
–	458	22.4	0.54	8.65	–	799	5.76	0.15	11.72
–	558	22.3	0.45	9.38	–	985	22.0	0.33	12.80
–	692	22.1	0.36	10.64	–	1138	21.8	0.28	13.60
–	989	22.0	0.24	12.50					
–	1133	22.0	0.22	13.46	Ca^{40}	191	4.67	0.56	6.00
					–	282	10.5	0.76	7.00
Ar^{40}	138	7.40	1.01	5.34	–	380	10.5	0.56	8.13
–	189	7.40	0.72	6.02	–	577	10.5	0.37	10.09
–	241	7.45	0.57	6.83	–	776	10.3	0.27	11.38
–	292	7.40	0.47	7.38	–	874	10.3	0.24	11.94

100 ~ 140 kev. For Ne^{20}, the values by Porat and Ramavataram are consistently some 20 per cent higher than the values reported here. For the remaining projectiles, no other empirical data exist in this energy range except those of ORMROD et al. which, in most cases, overlap our results at lower energies. For all projectiles except Al^{27}, our electronic stopping cross section results overlap within 10 per cent the findings of ORMROD et al. Our Al^{27} data are some 30 per cent higher. The results are shown in Fig. 5 a–5 h.

We have assumed that the electronic stopping cross sections can be fitted to an equation of the form $S_e = kE^p$. This assumption is justified by noting that in all but two instances, the log-log plot of S_e versus projectile energy yields a straight line. This type of energy dependence is predicted by theory with $p \approx 0.5$, although small deviations from $p \approx 0.5$ may occur

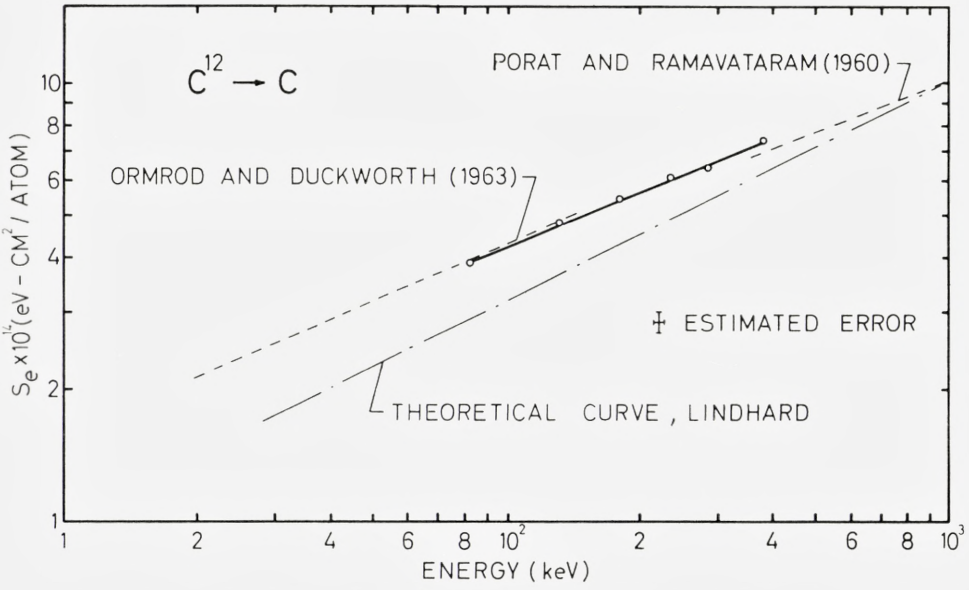

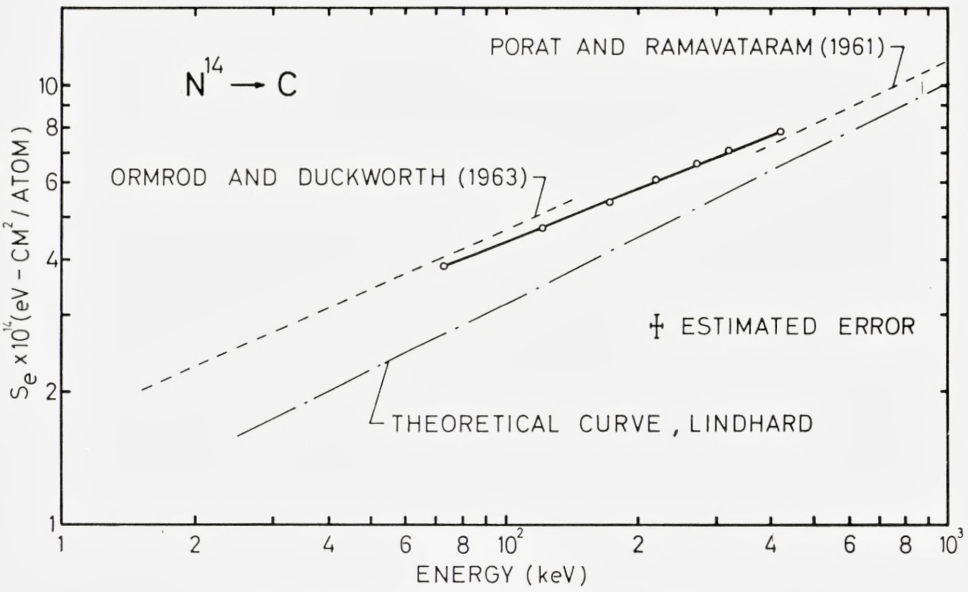

Figure 5a. Electronic stopping cross section S_e.

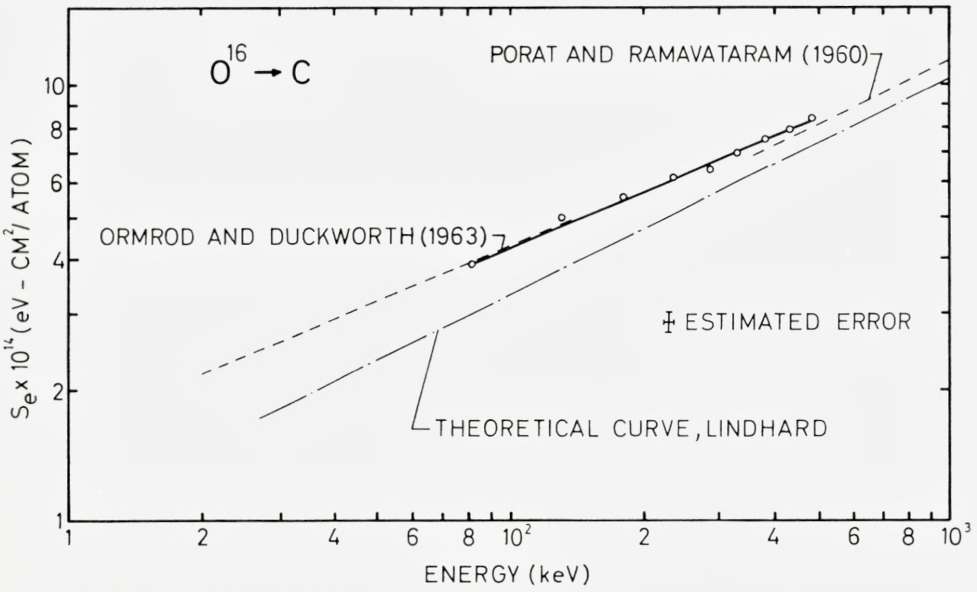

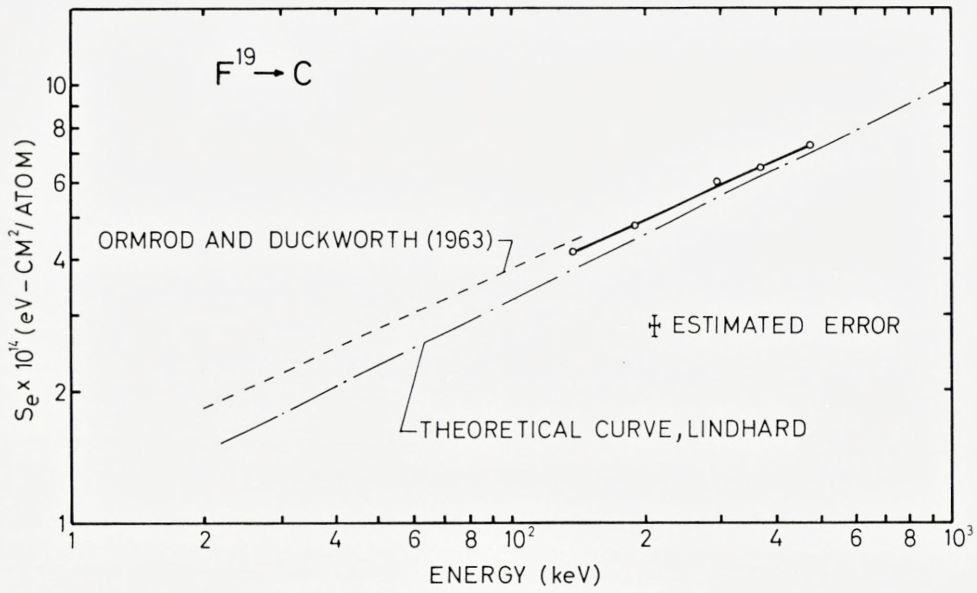

Figure 5b. Electronic stopping cross section S_e.

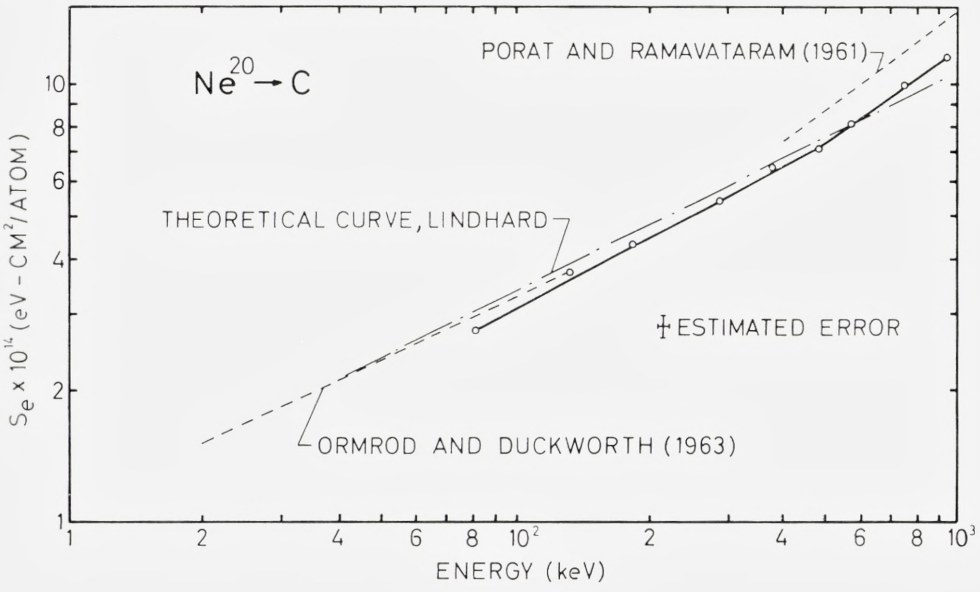

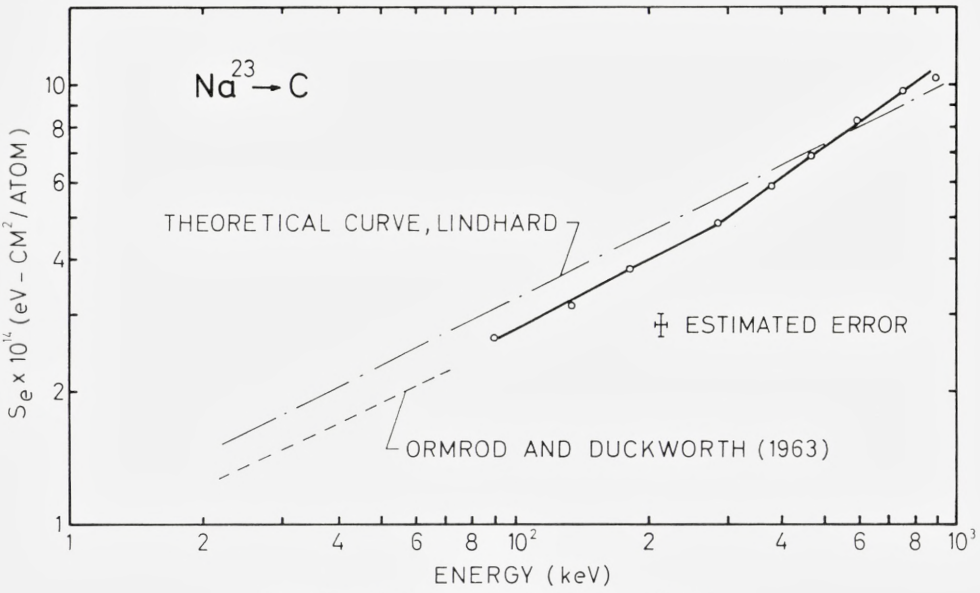

Figure 5c. Electronic stopping cross section S_e.

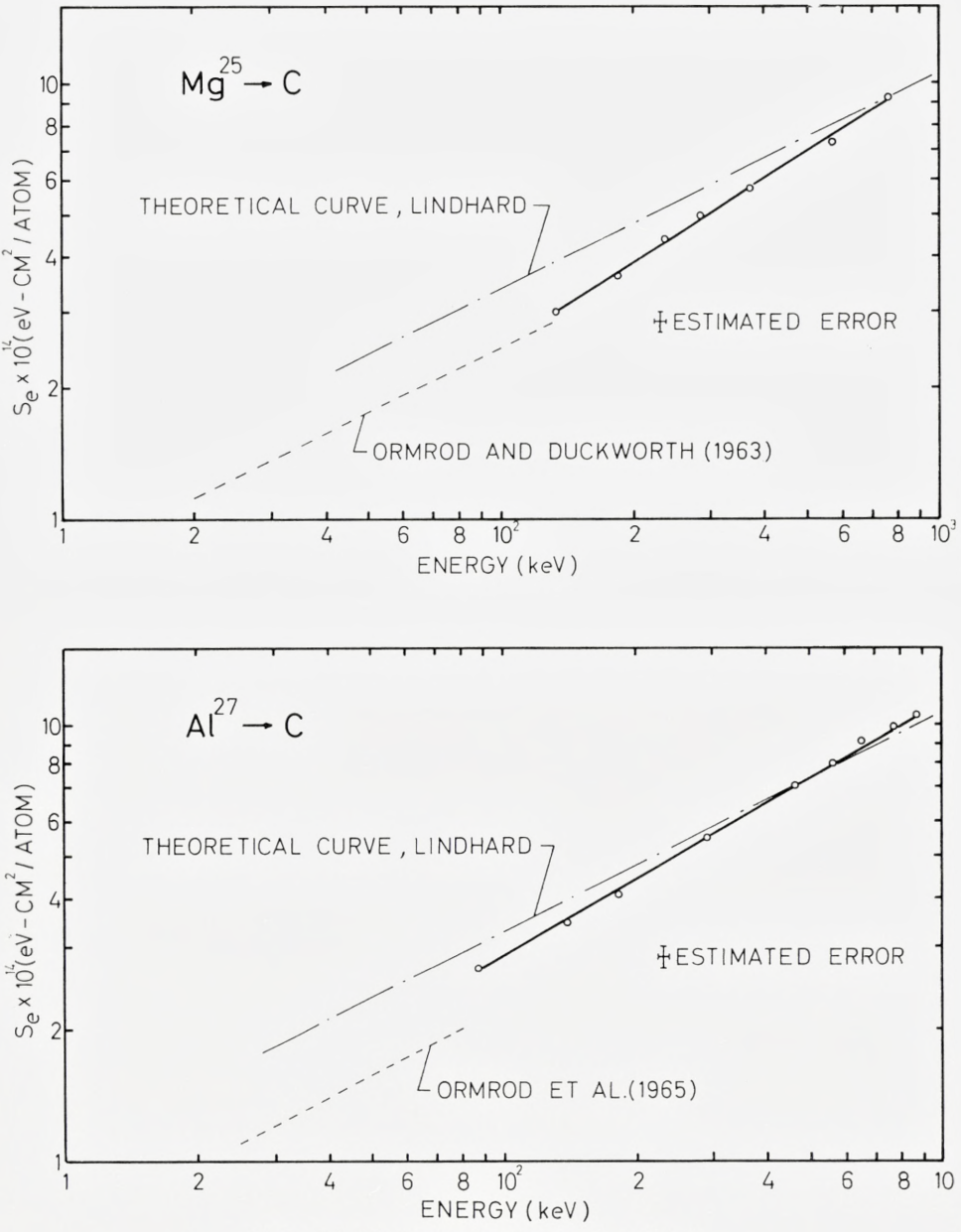

Figure 5d. Electronic stopping cross section S_e.

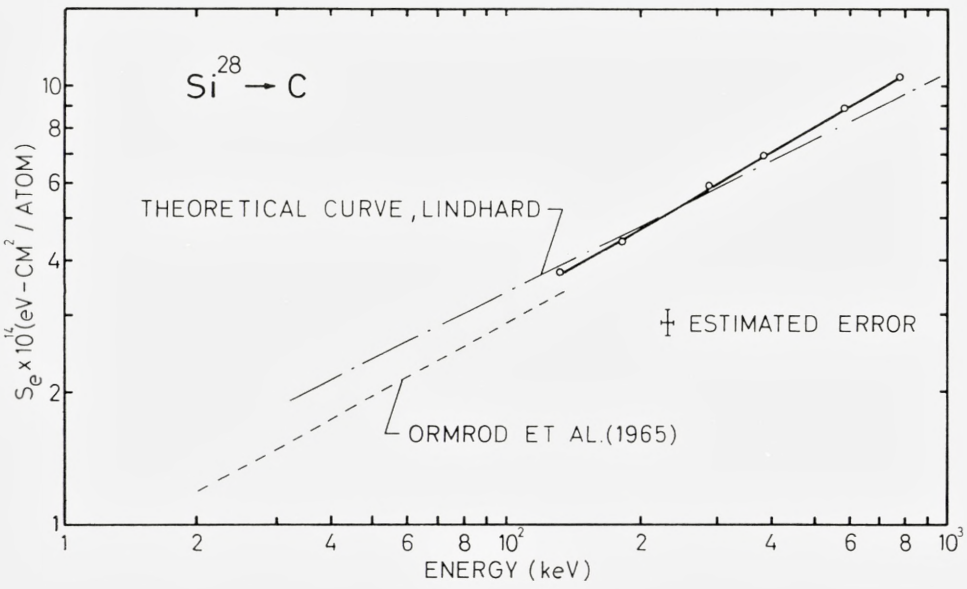

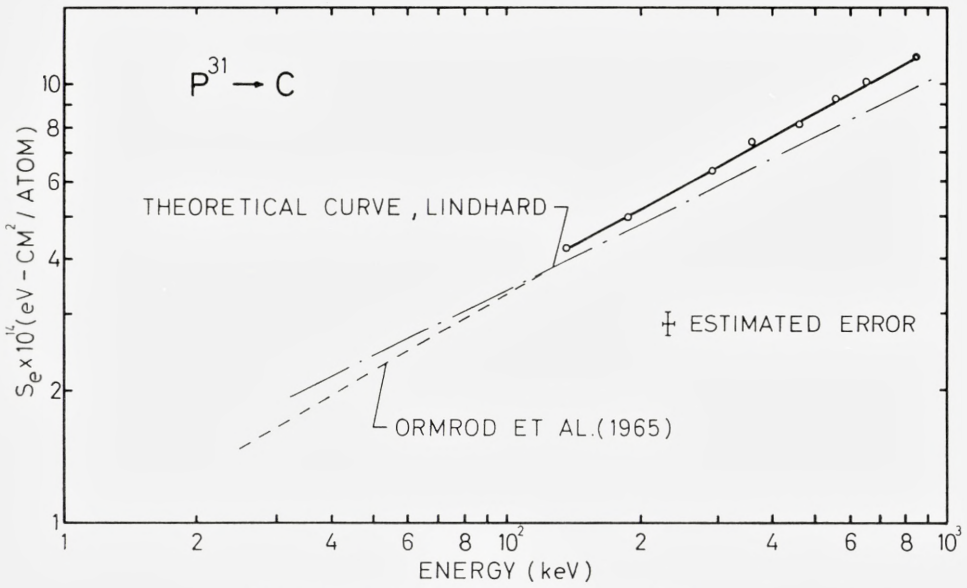

Figure 5e. Electronic stopping cross section S_e.

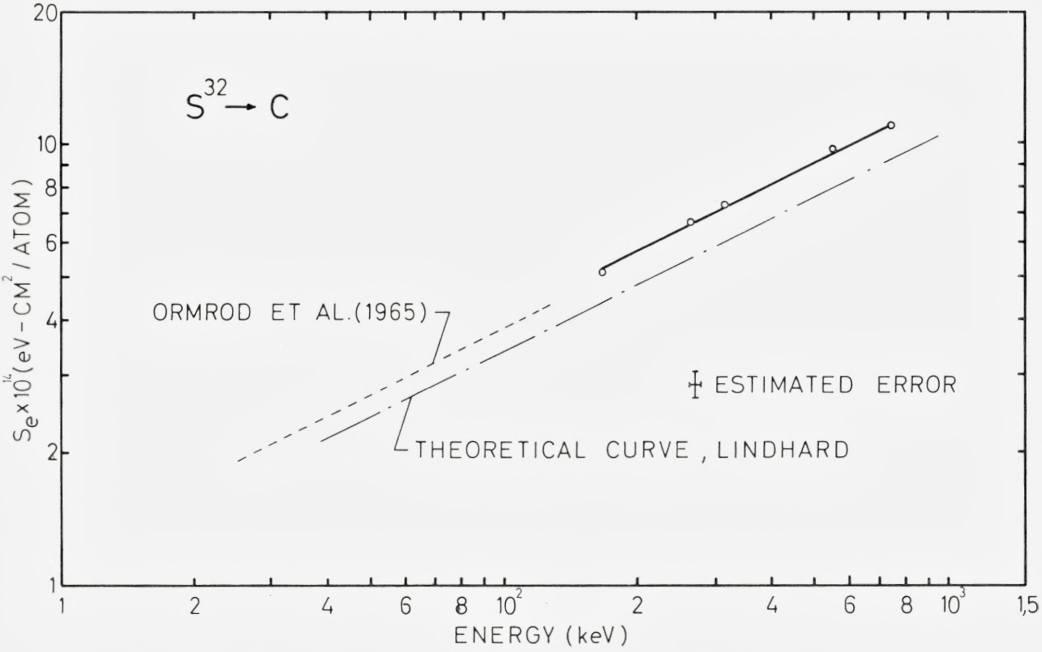

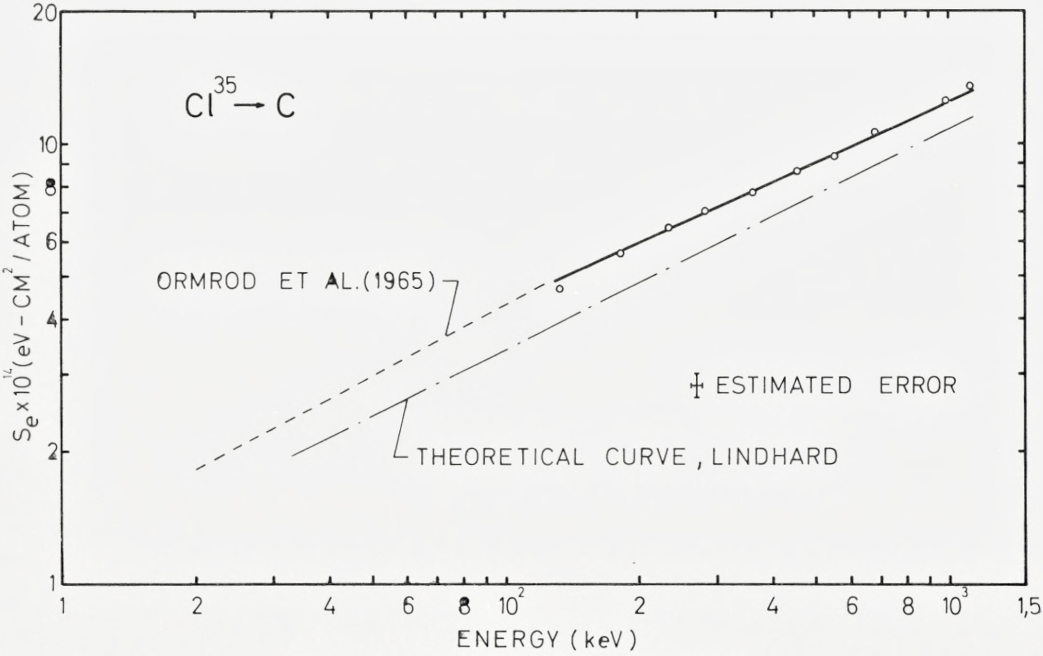

Figure 5f. Electronic stopping cross section S_e.

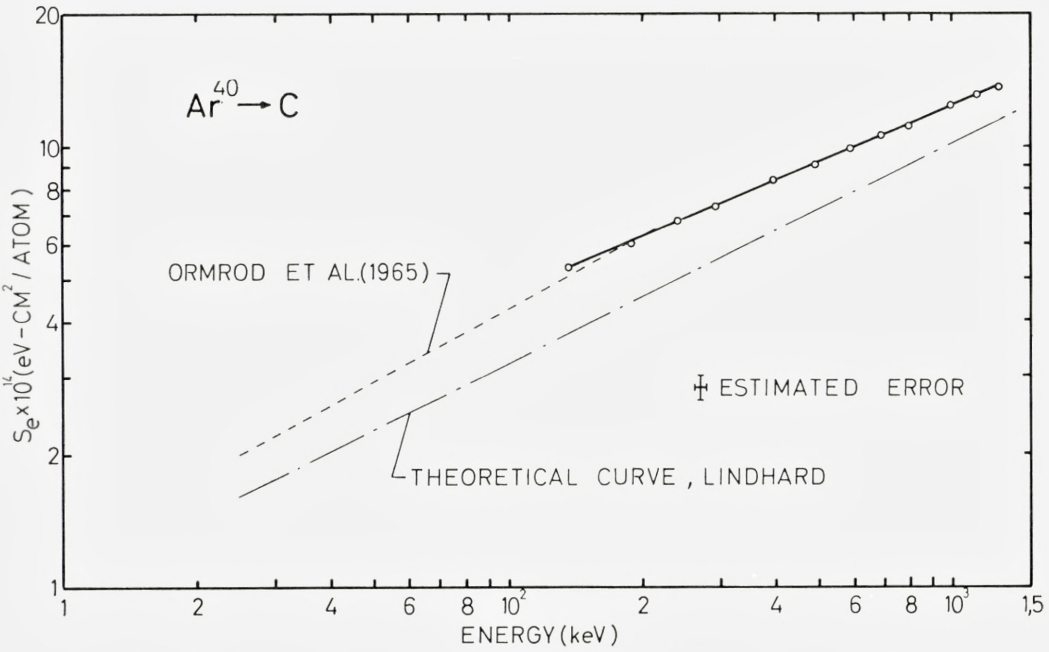

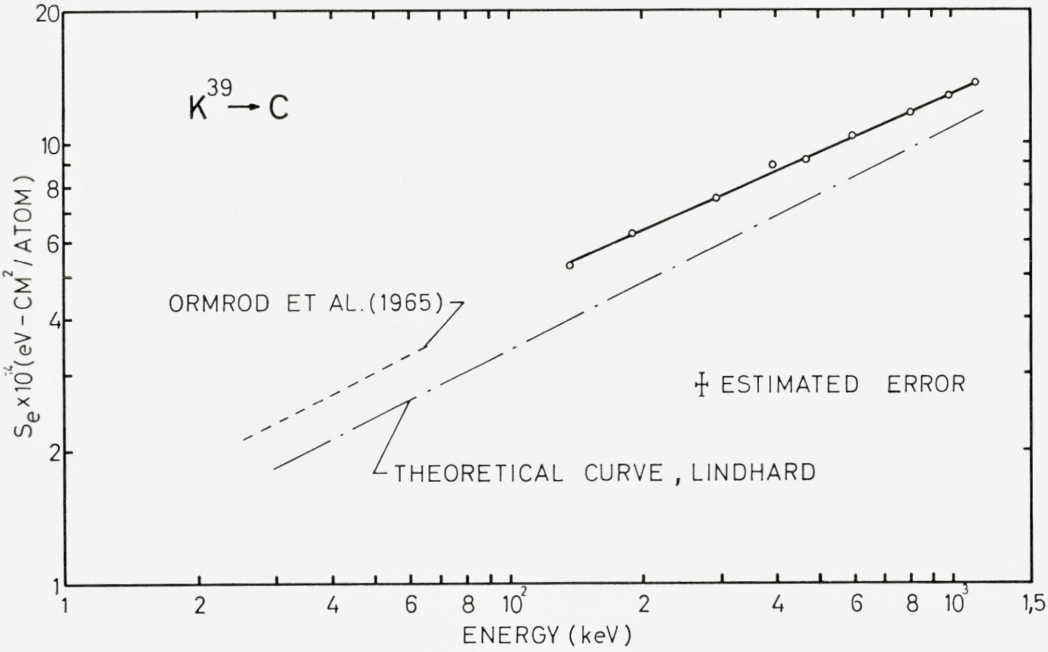

Figure 5g. Electronic stopping cross section S_e.

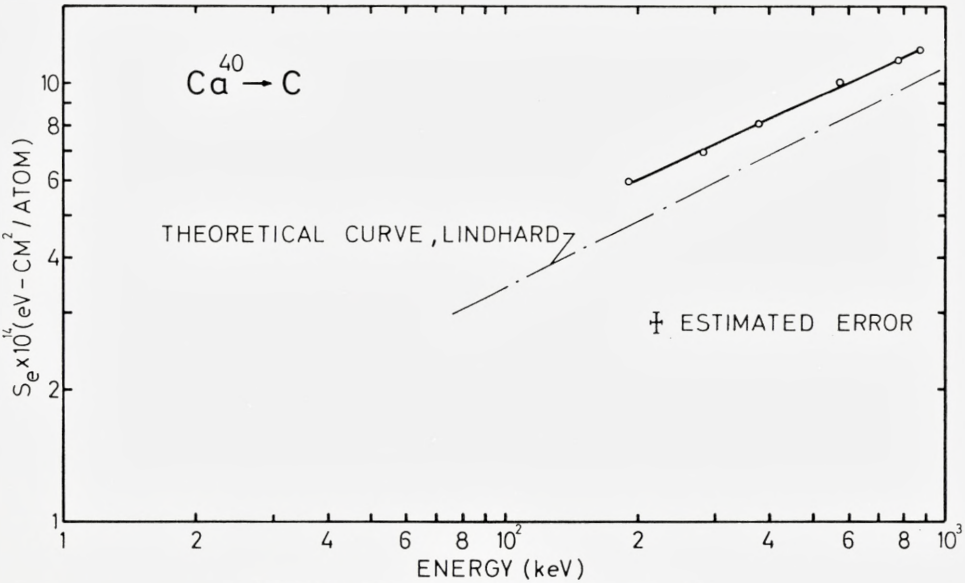

Figure 5h. Electronic stopping cross section S_e.

due to, for example, shell effects. Furthermore, in the cases where the nuclear correction S_n^* is negligible, i.e. for nearly all the data with $Z_1 < 10$, we find that the observed cross sections, $S_0 \approx S_e$, fit the above relationship. However, these remarks should not be taken as a proof that p is independent of the energy over a large energy range. In fact, our data suggest that p varies slowly with energy with an average not far from 0.5. In the cases of Ne^{20} and Na^{23}, a better fit is established by broken lines with two p-values for each element.

Plotted against Z_1 in Fig. 6 are the p-values obtained from this experiment and those found by ORMROD et al.[6] at lower energies. We have extracted p-values from PORAT and RAMAVATARAM'S[12] data in the case of $Z_1 = 6$, 7, 8, and 10. It is seen that with some correlation between adjacent elements, the empirical values exhibit an oscillation around $p = 0.5$ with an amplitude of about 0.1. As the energy ranges differ in the three experiments, differences outside those contributed by experimental errors would not be surprising.

In their treatment of their experimental data, ORMROD et al. found that, plotted against Z_1 for a constant, common projectile velocity of $v = 0.41\, v_0$, the electronic stopping cross sections exhibited a peculiar oscillation with a

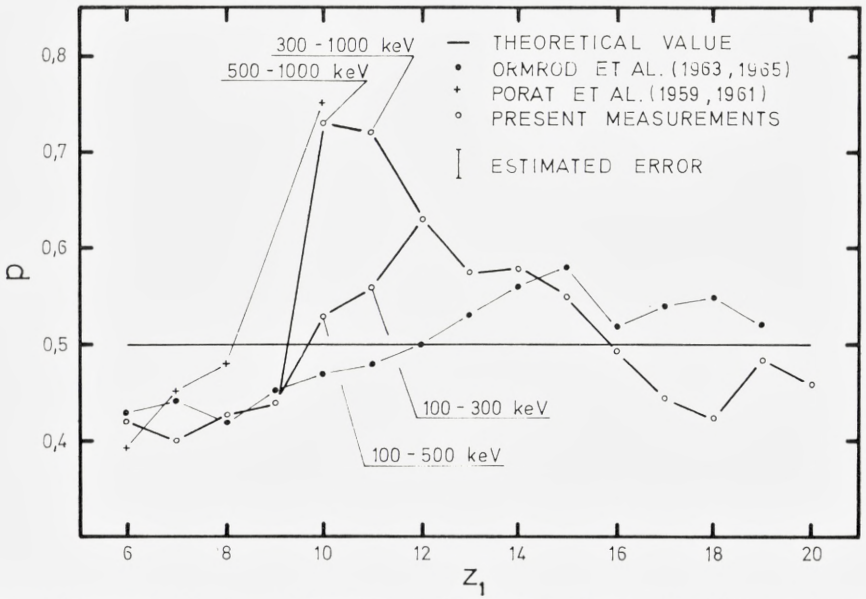

Figure 6. Exponent p in $S_e = k\,E^p$ against Z_1. The data by ORMROD et al.[6] cover the region below approx. 140 kev, the data by PORAT et al.[12] cover the region beyond 400 kev, when $Z_1 = 6$, 7, 8, and 10, and our data cover the region 100 to 500 kev when $6 \leq Z_1 \leq 9$, and 100 to 1000 kev when $10 \leq Z_1 \leq 20$. In the special cases, $Z_1 = 10$ and 11, two p-values have been displayed for each element.

long period around the curve predicted theoretically by LINDHARD and SCHARFF[5]. Due to our extended energy range, we have added three similar curves at different constant particle velocities, namely $\frac{v}{v_0} = 0.64$, 0.91, and 1.1. This makes it possible to study the periodicity in more detail. The results are displayed in Fig. 7 and compared with the theoretical curves by LINDHARD et al. The choice of a common velocity v is not strictly appropriate in the Thomas-Fermi treatment. Instead, we should have chosen a constant Thomas-Fermi velocity, i.e. constant $v \cdot Z_1^{-2/3}$. A closer examination of Fig. 7, however, shows that the qualitative features are not affected significantly if $v \cdot Z_1^{-2/3}$ is kept constant instead of v. In the same plot are also shown the theoretical stopping values by FIRSOV[4] as quoted by TEPLOVA et al.[14]. Based on a semi-classical Thomas-Fermi treatment, the results are given by

$$S_e = 5.15 \cdot 10^{-15}(Z_1 + Z_2)\frac{v}{v_0}\,\mathrm{ev} \cdot \mathrm{cm}^2/\mathrm{atom}.$$

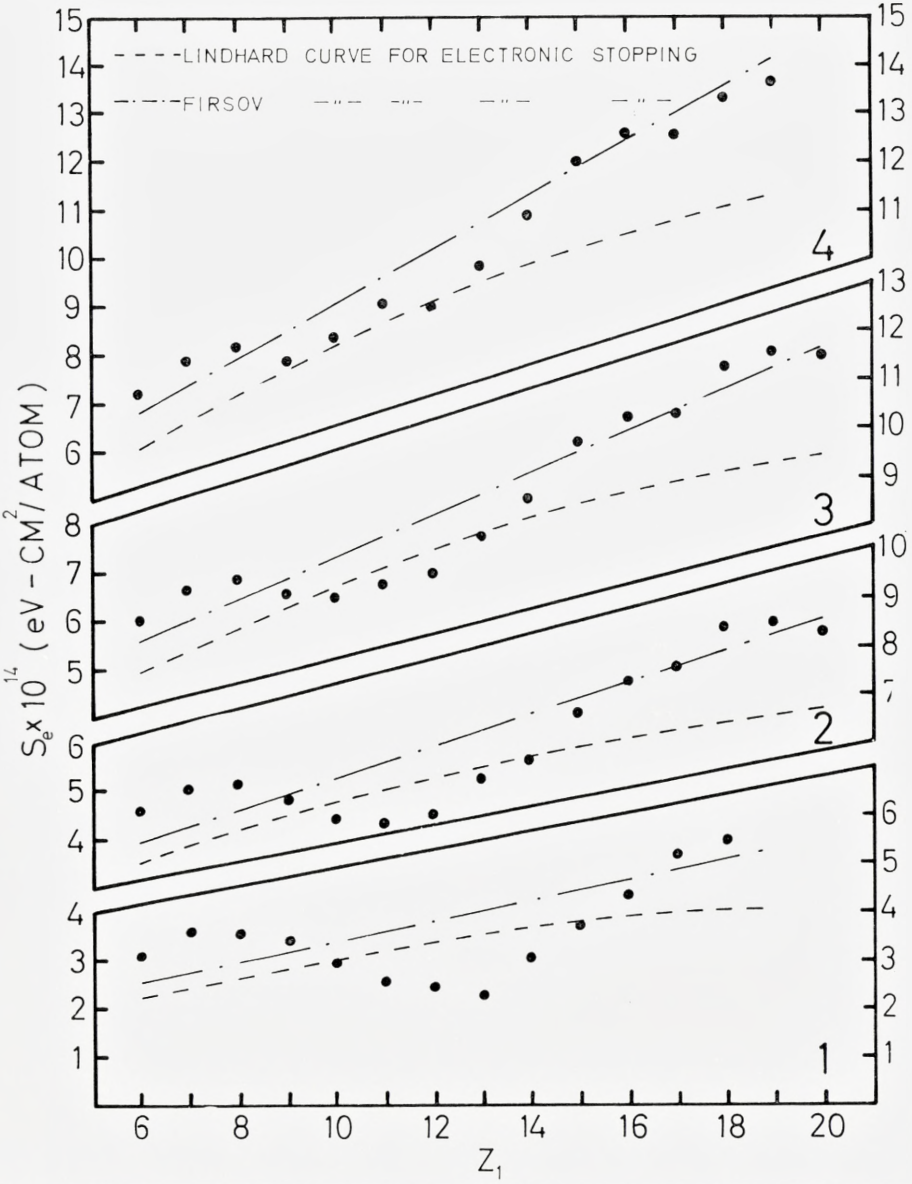

Figure 7. Electronic stopping cross section S_e versus Z_1 for constant common velocity. 1) $v = 0.41\ v_0$. 2) $v = 0.63\ v_0$. 3) $v = 0.91\ v_0$. 4) $v = 1.1\ v_0$. The data at $v = 0.41\ v_0$ are taken from Ormrod et al.[6]. Also shown are the theoretical curves by Lindhard and Scharff[5] and by Firsov[4].

Our data exhibit the same qualitative behaviour as the earlier empirical data[6]. However, a few observations can be made:

1) As would be expected, the relative amplitude of the oscillations tends to decrease with increasing particle velocity. Possible shell effects average out as a result of more close collisions where the electron clouds penetrate each other more deeply. It is observed that the simple oscillatory behaviour for small velocities is not maintained as the velocity increases. More complex structure appears.
2) The mean absolute deviation from the Lindhard theory is slightly larger at higher projectile velocities.
3) The reasonable agreement between Lindhard's and Firsov's predicted curves is partly due to the present selection of Z_1 values. Considering the functional dependence on Z_1 and Z_2 in the two theories, this is to be expected.

In the measurements, we have used singly charged ions for energies from 100 to 500 kev and doubly charged ions for energies from 500 to 1000 kev. In order to determine whether the energy loss depends on the charge state of either the incoming ions or the emerging ions from the foil, an experimental study was carried out.

a) With the analyzing magnet adjusted to one charge state, we studied the influence of the charge state of the incoming ions on the observed energy loss. We did not see any appreciable effect due to variation of the charge state of the incoming ions with the same kinetic energy. Assuming that the capture and the loss cross sections[13] in carbon for kev ions with $Z_1 < 20$ are greater than $2 \cdot 10^{-16}$ cm^2, the mean free path for obtaining charge equilibrium will be less than 0.1 μg/cm^2. This value is much smaller than the thickness of the thinnest foil (5 μg/cm^2) used in the present experiment.
b) The foil was bombarded with the same charge state ions. The dependence of the energy loss on the charge state of the emerging ions was studied. A few per cent difference between ΔE^+ and ΔE^{++} was observed where the charge index refers to the charge state of the emerging ions. The effect is of a statistical nature and partly stems from the different energy dependence of the capture and loss cross sections.

A more correct experimental procedure of taking stopping power data would be to average over the observed energy losses for different charge states of the outgoing ions, i.e.

$$\Delta E_0 = \frac{\sum_n I^{n+} \Delta E^{n+}}{\sum_n I^{n+}} ,$$

where I^{n+} is the flux of the outgoing ions in charge state $n+$.

As the charge state effect at the most is a few per cent, we have not proceeded with the more detailed measurements.

Acknowledgments

The authors wish to express their thanks to J. A. Davies and J. Lindhard for many stimulating discussions, to our colleagues, in particular to K. O. Nielsen, for their interest, to S. Olesen for his assistance in constructing the equipment, and to P. B. Kjær for operating the accelerator. This work was financially supported by the Danish State Research Foundation. One of the authors (C.A.S.) acknowledges the U.S. State Department for a Fulbright Travel Grant.

Appendix

Nuclear Stopping Correction

This appendix gives a general description of the analytical methods used for estimating the nuclear stopping contribution, S_n^*, encountered in the experiment. As previously mentioned in the Data Treatment section, it is a reasonable approximation to restrict our attention to the Gaussian-distributed nuclear collisions, i.e.

$$S_n^* = \int_0^{T^*} T d\sigma .$$

Here, T^* may be estimated from the equation

$$(T^*)^2 = (\Omega^*)^2 = N\Delta R \int_0^{T^*} T^2 d\sigma , \qquad \text{(A 1)}$$

where $N\Delta R$ is the number of atoms per cm^2, and $d\sigma$ is the differential cross section for an energy transfer T.

To solve eq. (A 1) with respect to T^*, it is convenient to introduce the reduced path length and the reduced energy, cf. LINDHARD et al.[9], ϱ and ε respectively:

$$\varrho = NRM_2 4\pi a^2 \frac{M_1}{(M_1+M_2)^2},$$

and

$$\varepsilon = E \frac{aM_2}{Z_1 Z_2 e^2 (M_1+M_2)},$$

where $a = a_0\ 0.8853(Z_1^{2/3}+Z_2^{2/3})^{-1/2}$ is the screening distance of the ion-atom potential.

If the interaction potential obeys certain similarity relations, LINDHARD et al. have shown that the differential cross sections may be written in the form

$$d\sigma = \pi a^2 \frac{dt}{2t^{3/2}} f(t^{1/2}), \tag{A 2}$$

where $t^{1/2} = \varepsilon \sin\frac{\theta}{2} = \varepsilon \sqrt{\frac{T}{T_{\max}}}$, θ is the scattering angle in the center of mass system, and $f(t^{1/2})$ depends on the chosen potential.

Equation (A 2) applies for power potentials as well as for screened potentials such as the Thomas-Fermi potential.

Combining eqs. (A 1) and (A 2), we get

$$F(\varepsilon^*) = \frac{\int_0^{\varepsilon^*} t f(t^{1/2})\, dt^{1/2}}{(\varepsilon^*)^4} = \frac{1}{N\Delta R \pi a^2}, \tag{A 3}$$

where $\varepsilon^* = \varepsilon \sqrt{\frac{T^*}{T_{\max}}}$.

Once $f(t^{1/2})$ is specified by selecting a convenient potential, ε^* and T^* may be evaluated from eq. (A 3) when the thickness of the film and the ion-atom combination (Z_1, Z_2) are known. It should be noted that ε^* does not depend on energy, while T^* is inversely proportional to the square root of energy.

Applying the relation

$$\left(\frac{d\varepsilon}{d\varrho}\right)_n^* = \int_0^{\varepsilon^*} f(t^{1/2}) \frac{1}{\varepsilon}\, dt^{1/2} = \int_0^{\varepsilon^*} f(t^{1/2}) \frac{1}{\varepsilon^*}\left(\frac{\varepsilon^*}{\varepsilon}\right) dt^{1/2},$$

the following result for the Gaussian nuclear stopping cross section is obtained:

$$S_n^* = 2.57 \cdot 10^{-16} \frac{A_1 Z_1^2 Z_2^2 \varepsilon^*}{A_2 E} I(\varepsilon^*) \text{ ev} \cdot \text{cm}^2/\text{atom}. \qquad \text{(A 4)}$$

The energy E is measured in kev, and $I(\varepsilon) = \dfrac{d\varepsilon}{d\varrho} = \displaystyle\int_0^{\varepsilon} f(t^{1/2}) \frac{1}{\varepsilon} dt^{1/2}$ is the stopping cross section in the reduced units.

Equation (A 4) exhibits some peculiar features:

(a) The Gaussian nuclear stopping cross section is inversely proportional to the energy as ε^* is independent of the energy.
(b) Change of the applied potential within the framework of eq. (A 2) alters the value of ε^* according to eq. (A 3), but does not abolish the inverse proportionality with the energy.

Strictly speaking, formula (A 1) applies only when the energy loss is much smaller than the energy of the beam, i.e. $\Delta E_0 \ll E_i$. In the case of thicker films, $\Delta E_0 \lesssim E_i$. LINDHARD and NIELSEN[15] have given a more rigorous formula.

Institute of Physics,
University of Aarhus, Denmark
B. Fastrup, P. Hvelplund,
*and C. A. Sautter**)

---

*) Present address: *Physics Department, Concordia College Moorhead, Minnesota, U.S.A.*

References

(1) N. Bohr, Phil. Mag. **25**, 10 (1913).
N. Bohr, Mat. Fys. Medd. Dan. Vid. Selsk. **18**, 8 (1948).
(2) E. Fermi and E. Teller, Phys. Rev. **72**, 399 (1947).
(3) J. Lindhard, Mat. Fys. Medd. Dan. Vid. Selsk. **28**, 8 (1954).
(4) O. B. Firsov, Soviet Phys. JETP **9**, 1076 (1959).
(5) J. Lindhard and M. Scharff, Phys. Rev. **124**, 128 (1961).
(6) J. H. Ormrod and H. E. Duckworth, Can. J. Phys. **41**, 1424 (1963).
J. H. Ormrod, J. R. Macdonald, and H. E. Duckworth, Can. J. Phys. **43**, 275 (1965).
(7) E. Bøgh, P. Dahl, H. E. Jørgensen, and K. O. Nielsen: A 600 kV Heavy Ion Accelerator with Magnet for Isotopical Separation. Preprint (1965). To be published.
(8) E. J. Williams, Proc. Roy. Soc. **A 125**, 420 (1929).
(9) J. Lindhard, M. Scharff, and H. E. Schiøtt, Mat. Fys. Medd. Dan. Vid. Selsk. **33**, 14 (1963).
(10) C. A. Sautter and E. J. Zimmermann, Phys. Rev. **140**, A 490 (1965).
(11) R. D. Moorhead, J. Appl. Phys. **36**, 391 (1965).
(12) D. I. Porat and K. Ramavataram, Proc. Roy. Soc. **A 252**, 394 (1959), Proc. Phys. Soc. **77**, 97 (1961), Proc. Phyc. Soc. **78**, 1135 (1961).
(13) V. S. Nikolaev, Soviet Phys. USPEKHI **8**, 269 (1965).
(14) Ya. A. Teplova, V. S. Nikolaev, I. S. Dmitriev, and L. N. Fateeva, Soviet Phys. JETP **15**, 31 (1962).
(15) J. Lindhard and V. Nielsen, Phys. Letters **2**, 209 (1962).

Indleveret til Selskabet den 12. maj 1966.
Færdig fra trykkeriet den 8. december 1966.